

# Small Body Simulations for Navigation Approach and Landing

Robert W. Gaskell\*

*Jet Propulsion Laboratory, California Institute of Technology, 4800 Oak Grove Drive, Pasadena, CA, 91109*

**Small body simulations have played a significant role in the planning and development of many recent missions to asteroids and comets. As closer approaches, and ultimately landings, are attempted, it will become necessary to simulate the surfaces of these bodies to increasingly high resolutions. Techniques for doing this, originally developed for Mars surface simulations, are being extended to generate artificial small body topography to arbitrarily high resolution.**

## Nomenclature

$A$	=	Interim surface label
$c$	=	crater distribution exponent
$d$	=	crater diameter
$D$	=	stochastic amplitude
$i, j$	=	fundamental surface labels
$I, J$	=	level specific surface labels
$F$	=	face number
$K$	=	face/level index
$L$	=	level index
$N$	=	counter
$R$	=	chaotic function
$S$	=	level spacing
$T$	=	Tag array index
$\mathbf{v}$	=	surface vector
$\mathbf{w}$	=	generic vector
$w$	=	magnitude of $\mathbf{w}$
$\mathbf{n}$	=	unit normal vector
$\Phi$	=	crater density

## 1. Introduction

Years before the NEAR spacecraft approached Eros for the first time, optical navigators at JPL were analyzing images of the asteroid in order to determine the spacecraft's orbit. Before the impactor on board Deep Impact detached from the spacecraft and headed toward comet Tempel 1, its software had already taken the same journey millions of times. Similar simulations were carried out in preparation for Stardust and Deep Space 1 encounters, and more recently for Hayabusa's upcoming encounter with Itokawa and Dawn's 2011 encounter with Vesta.

All of these spacecraft had their initial encounters with small bodies that were created from the software described below. Instead of the typical few hundred thousand vector model that most simulations use, these models have, potentially, almost  $7 \times 10^{18}$  vectors. Of course, not all of the body needs to be constructed at any given time. To render a typical image, for example, a few million vectors will suffice, covering the entire body if the resolution is low enough or defining a restricted surface patch at high resolution.

The significant feature of these models is that whatever portion of the surface is created, and at whatever resolution, the vectors are the same as they would have been had the full set of vectors been generated. This is

---

\* Senior Engineer, Optical Navigation Group, JPL/CALTECH MS 301/150, 4800 Oak Grove Drive, Pasadena, CA 91001. AIAA Member.

accomplished by sorting the vectors into "levels", with a higher level vector array having lower resolution. The generation of a vector at a given level depends only on those at higher level. A second important feature is that stochastic processes are based on chaotic functions of position. Random variations at one point are completely independent of those at a neighboring point. This technique is a three dimensional extension of a Mars simulator<sup>1,2</sup> that has been used in Pathfinder and MER landing and roving studies.

Section 2 discusses the labeling scheme that allows small portions of the surface to be constructed with complete consistency. Section 3 describes the shape models that are the inputs for the small body simulations. Section 4 treats the addition of high-resolution topography, including craters rocks and fractal surfacing. Section 5 presents a few examples of the current applications of the techniques.

## 2. Labeling Scheme

The vectors of the models are labeled by grid points ( $i,j = 0,2^{30}$ ) on the six faces of a cube ( $f=1,6$ ). This automatically defines their connectivity, with edge and corner points common at adjoining faces. Each vector labeled by  $i,j,f$  is assigned a level, from 1 to 61, according to the following rule: If  $i$  contains  $p$  factors of 2, and  $j$  contains  $q$  factors of 2, then its level  $L$  is

$$L(i,j) = \begin{cases} 2p+2 & (p=q) \\ 2p+1 & (p<q) \\ 2q+1 & (p>q) \end{cases} \quad (1)$$

For a corner point,  $i=0$  or  $2^{30}$  and  $j=0$  or  $2^{30}$ , the level is 61. The grid below shows the highest-level points:

<b>61</b>	<b>55</b>	<b>57</b>	<b>55</b>	<b>59</b>	<b>55</b>	<b>57</b>	<b>55</b>	<b>61</b>
<b>55</b>	<b>56</b>	<b>55</b>	<b>56</b>	<b>55</b>	<b>56</b>	<b>55</b>	<b>56</b>	<b>55</b>
<b>57</b>	<b>55</b>	<b>58</b>	<b>55</b>	<b>57</b>	<b>55</b>	<b>58</b>	<b>55</b>	<b>57</b>
<b>55</b>	<b>56</b>	<b>55</b>	<b>56</b>	<b>55</b>	<b>56</b>	<b>55</b>	<b>56</b>	<b>55</b>
<b>59</b>	<b>55</b>	<b>57</b>	<b>55</b>	<b>60</b>	<b>55</b>	<b>57</b>	<b>55</b>	<b>59</b>
<b>55</b>	<b>56</b>	<b>55</b>	<b>56</b>	<b>55</b>	<b>56</b>	<b>55</b>	<b>56</b>	<b>55</b>
<b>57</b>	<b>55</b>	<b>58</b>	<b>55</b>	<b>57</b>	<b>55</b>	<b>58</b>	<b>55</b>	<b>57</b>
<b>55</b>	<b>56</b>	<b>55</b>	<b>56</b>	<b>55</b>	<b>56</b>	<b>55</b>	<b>56</b>	<b>55</b>
<b>61</b>	<b>55</b>	<b>57</b>	<b>55</b>	<b>59</b>	<b>55</b>	<b>57</b>	<b>55</b>	<b>61</b>

**Figure 1. Highest-level grid points.**

The vector at a point is directly determined by its higher-level neighbors, on the diagonals for even level points and horizontally and vertically for odd level points. These are called a point's parents. A point on an edge, which always has an odd level, has one parent on another face. The set of points which ultimately generate a point are called its ancestors,

The array represented by Fig. 1 is very sparse, 81 elements in a  $2^{30}+1$  square array. For this reason, a separate array is specified for each level. The space of a level is defined by

$$S(L)=2^{\lfloor(L-1)/2\rfloor} \quad (2)$$

where  $\lfloor x \rfloor$  represents the integral part of  $x$ . The new array is labeled by  $I,J$  where  $i=SI$ ,  $i=SJ$  are the indices of the old array. For an odd level, one of  $I,J$  is odd, and the other even, while for an even level, both  $I$  and  $J$  are odd. The exception is  $L=61$ , the corner points, where  $I=0,1$  and  $J=0,1$ .

The natural limits for a level  $L$  array are  $I, J=0, 2^{30}/S(L)$ . If only a portion of the surface is to be generated, down to some level  $L_0$ , then the limits are more restrictive. Since there are six faces to the cube, a new label is introduced,

$$K=F+6(L-1) \quad (3)$$

where the faces  $F$  are numbered from 1 to 6. For the six  $K$  at level  $L_0$ , some external constraint, such as a camera field of view, determines the minimum and maximum values of  $I$  and  $J$ ,  $I_{\min}(K)$ ,  $I_{\max}(K)$ ,  $J_{\min}(K)$ ,  $J_{\max}(K)$ . If the constraint excludes all level  $L_0$  vectors on a face, the minimum is set to 0, and the maximum to -1. The same null limits are set for lower levels,  $L < L_0$ . Limits for  $L > L_0$  are determined recursively, by finding the set of parents of all points of a given level and determining its index domain. Notice that even if there are no level  $L_0$  points on a face, there will be some higher level points because eventually, as the recursion proceeds, a parent of a point on one face will lie on an adjoining face.

Once the limits for each array have been determined, for all  $K$  from 1 to 366, the number of possible points is specified by

$$N(K) = (I_{\max}(K) - I_{\min}(K) + 1)(J_{\max}(K) - J_{\min}(K) + 1) \quad (4)$$

This is actually an over-estimate, by a factor of about 2 for odd levels and a factor of about 4 for even levels. An intermediate label is determined from the  $N$  according to

$$A(I, J, K) = N(K+1) + (I - I_{\min}(K))(J_{\max}(K) - J_{\min}(K) + 1) + (J - J_{\min}(K) + 1) \quad (5)$$

where  $N(367)=0$ . Since only about one third of these labels represent an actual grid point, a modified tag  $T$  is determined by counting the number of actual points as  $A$  increases.  $T(A)$  is zero if  $A$  does not correspond to a valid point, and if  $A$  is a valid point then  $T(A)$  equals the number of valid points with a label less than or equal to  $A$ . If  $L_K$  is the level corresponding to  $K$  from Eq. (3), then the validity condition is

$$L_K = L(I * S(L_K), J * S(L_K)) \quad (6)$$

The tag  $T$  is used to label all quantities defining the simulated surface, such as vectors, albedo, and fractional rock coverage.

### 3. Initialization of the Shape Model

The initial shape model defining a small body consists of a set of vectors labeled as described above, with an odd minimum level  $L_0$  and the natural limits on  $I$  and  $J$  of  $0, q=2^{30}/S(L_0)$ . With the ancestors included, this represents a  $6q^2+2$  vector model after duplicate vectors on the edges have been eliminated. A frequent choice is  $q=512$ , leading to a 1.57 million vector initial model. This is the standard form for high-resolution shape models being produced by applying stereo-photoclinometry (SPC)<sup>3-7</sup> to imaging data.

Other initial shape models are re-sampled to fit this format by projecting them onto unit vectors defined by grid points on the faces of a cube. This can result in an uneven distribution of points on the surface. Once this initial model is found, a new set of direction vectors is constructed by stretching the cube into a rectangular solid with edges  $a$ ,  $b$ , and  $c$ , and shifting the center by an offset vector  $O$ . These parameters are chosen in order to equalize the surface areas of the shape model corresponding to each of the six faces. The resulting distribution is shown in Fig. 3a. The intersections of the grid lines within each face are then deformed in order to most nearly equalize the surface area projections of the cells on that face. The revised distribution is illustrated in Fig. 3b.

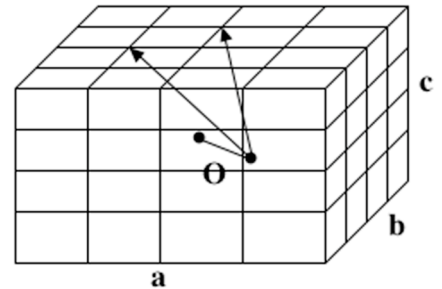
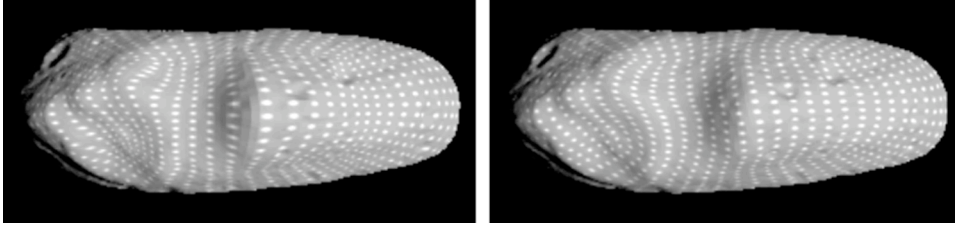


Figure 2. Initial direction vectors.



**Figure 3. Distributions after a) face area equalization, b) cell area equalization.**

If the resolution of the initial model is sufficient, then the surface generation algorithms are applied to the existing set of points. If a high-resolution sub-area is desired, then initial points are determined from stochastic interpolation between the existing points. The process proceeds from high level to low, starting at level  $L_0-1$ . If the new point is at  $i,j$  in the fundamental array, then its parents are at  $i\pm S(L),j$  and  $i,j\pm S(L)$  if its level  $L$  is odd, or at  $i\pm S(L),j\pm S(L)$  if  $L$  is even. If  $\mathbf{v}_k$  ( $k=1,4$ ) are the vectors defining four parent points, arranged in clockwise order as seen from above, then the unit normal  $\mathbf{n}$  to the surface is in the direction of  $\mathbf{w}=(\mathbf{v}_3-\mathbf{v}_1)\times(\mathbf{v}_4-\mathbf{v}_2)=\mathbf{n}\mathbf{w}$ , and the vector to the new point is

$$\mathbf{v} = (\mathbf{v}_1+\mathbf{v}_2+\mathbf{v}_3+\mathbf{v}_4)/4 + D(\sqrt{(w/2)})R(i,j)\mathbf{n} \quad (7)$$

where  $D$  is a scale-dependent stochastic amplitude.  $R$  is a random function that varies between  $(-1,1)$ . It is a chaotic function of position, in the sense that each point  $i,j$  on the fundamental grid has its own generator, completely independent from neighboring points.

#### 4. Construction of the topography

The topography is constructed by successively applying a series of processes, attempting to mimic the geological history of the surface. The small body generator is not as mature as the Mars simulator<sup>1,2</sup>, in the sense that fewer processes are available. However, it is more advanced in the sense that it is closer to being three dimensional. It is a true vector representation, rather than simply describing height as a function of horizontal location. The basic processes include fractal surfacing, cratering, and rock distribution. The last can be used to add large lumps to an initial body to mimic accretion. The simplest process is surfacing, which is accomplished by the stochastic interpolation described above. The only difference is that the second term in Eq. 7 is added to a pre-existing vector, rather than the average of the parents vectors.

The addition of rocks and craters is a level-dependent process, so that sub-resolution features are not included. Notice that odd level points form a diagonal array that, with the extension to other faces, completely covers the body. A rock or crater center is randomly placed within one of the cells, such as at the point  $\mathbf{x}$  in Fig. 4. Its size must be small enough that it not extend beyond the adjoining cells, and large enough that it cannot be accommodated in the same way in a lower odd-level array. The number of rocks or craters added is determined by the appropriate distribution function, measuring the number per unit area with sizes in the appropriate range. For craters, a power law is used<sup>8,9</sup>:

$$\Phi(d) = \Phi(d_0)(d/d_0)^{-c} \quad (8)$$

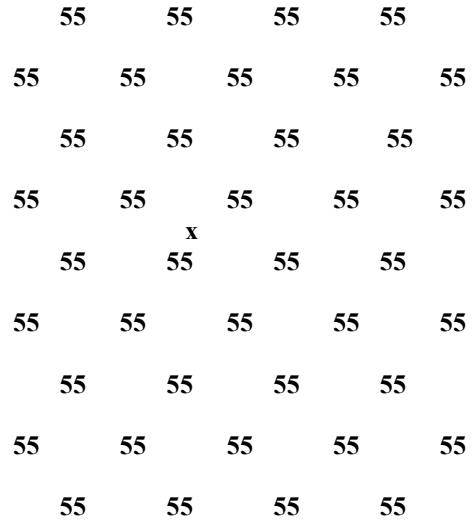


**Figure 4. Odd-level grid points.**

where  $\Phi$  represents the number of craters per square kilometer with diameter greater than  $d$ . The exponent  $c$  is typically in the range from 2 to 4. The rock distribution is determined from Golombek's model<sup>10</sup>, and varies with fractional surface coverage.

Once the center has been chosen, the topography corresponding to the feature is added. Rocks are elliptical in shape, with a randomly varying eccentricity and a height varying with fractional coverage according to the Golombek model. Small craters are bowl shaped, but larger ones acquire a flattened bottom. New surface is then added by stochastic interpolation. This process is carried out sequentially for rocks, from high levels to low. For craters, the centers are determined, and a random clock time is determined. Then the cratering is done according to the clock time, so that small craters can appear inside large ones, or large craters can obliterate small ones. A similar delay is used for rocks in the Mars model. The fractional rock coverage is carried through the calculation as a function of position, just like albedo and surface height. It can change, being reset to zero after a crater impact, but then increased as the crater ejecta produces more rocks. Only at the end are the actual rocks constructed.

## 5. Examples

There have been several close proximity missions recently, for which high-resolution simulations of the imaging data has proven useful. Next month, the Japanese spacecraft Hayabusa will encounter asteroid 25143 Itokawa. It will hover about 20 km away for several weeks. In October it will move in to 7 km, making further observations. Then, in November, it will touch down twice, taking samples to return to Earth. A series of several hundred images of a simulated Itokawa was studied to test how well SPC techniques could reproduce the shape and surface topography, and how well landmark optical navigation could predict the spacecraft trajectory during proximity navigation. The simulated asteroid, shown in Fig. 5, was based on a radar model<sup>11</sup> of Itokawa, with added craters, rocks and fractal surfacing. This is a small asteroid, only about 600 meters in its longest dimension. The simulation<sup>7</sup> demonstrated that landmark navigation techniques will be able to locate the spacecraft to about 50 cm during approach.

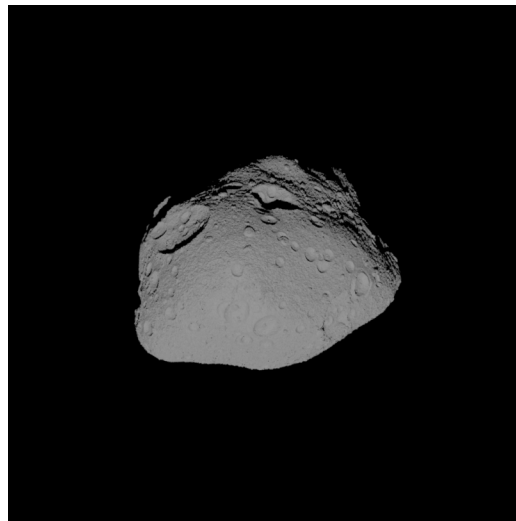


**Figure 5. Simulated asteroid Itokawa.**

Another simulation, for asteroid 4 Vesta, is shown in Fig. 6. This is based on a shape model<sup>12</sup> constructed from Hubble Space Telescope data, with added craters and fractal surfacing. Rocks were not added, since they will be sub-resolution. Vesta is about a thousand times larger than Itokawa, about 600 km in diameter. Notice the flattened bottoms of the larger craters. This simulation is being used in Dawn development studies.

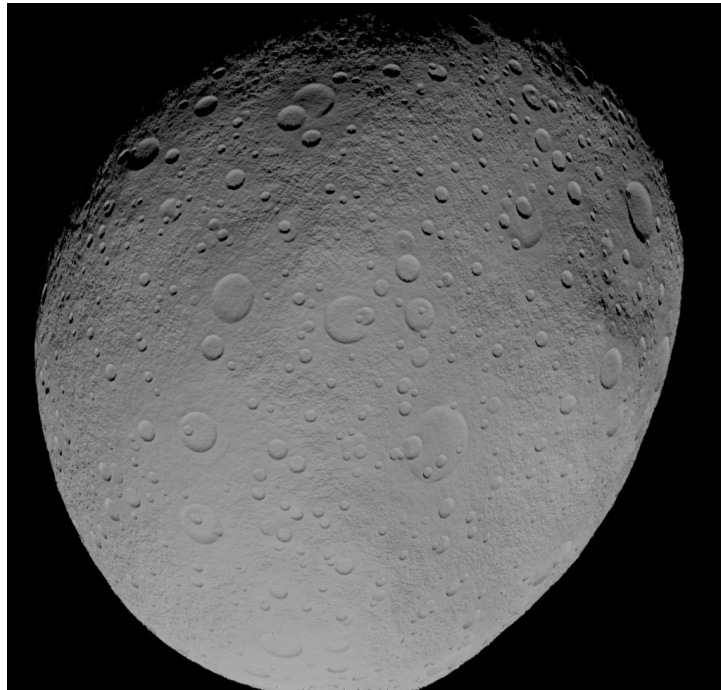


**Figure 6. Simulated asteroid Vesta.**

The final example is based on a 1.57 million vector model of Phobos<sup>5</sup> determined from SPC. Fig. 7a shows an image of the shape model corresponding to Viking Orbiter image 343A15. Notice the small craters that have been added by the simulation. Although the image resolution is 8 m/pixel, the global model only has a resolution of 30 m/pixel. Fig. 7b shows the central portion of the image, zoomed in by a factor of 4 and showing further detail from the simulation. Only a small portion of the surface was generated to produce this image.

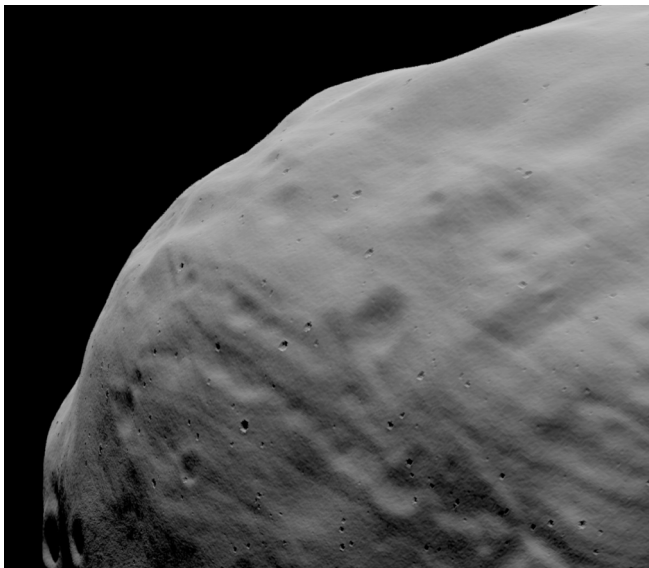


**Figure 7. Phobos shape model with added topography**

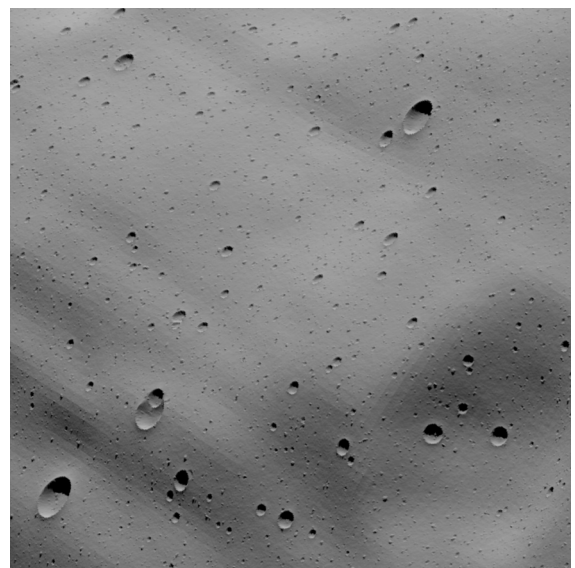


**Figure 8. Central region at 2 m/pixel resolution**

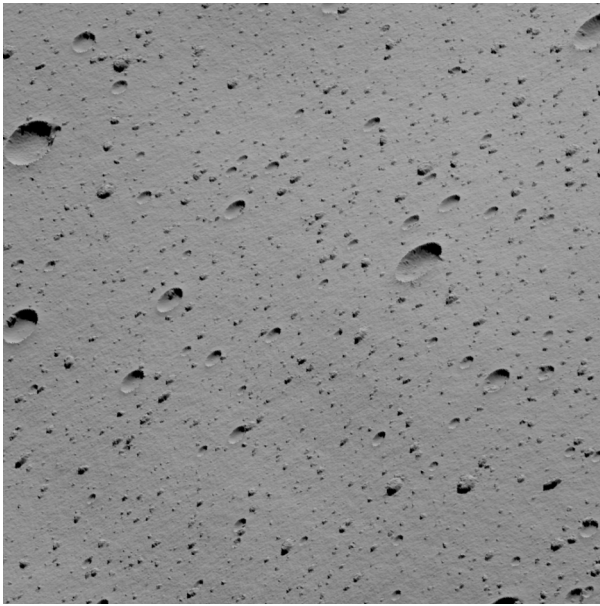


**Figure 9. Central region at 50 cm/pixel**

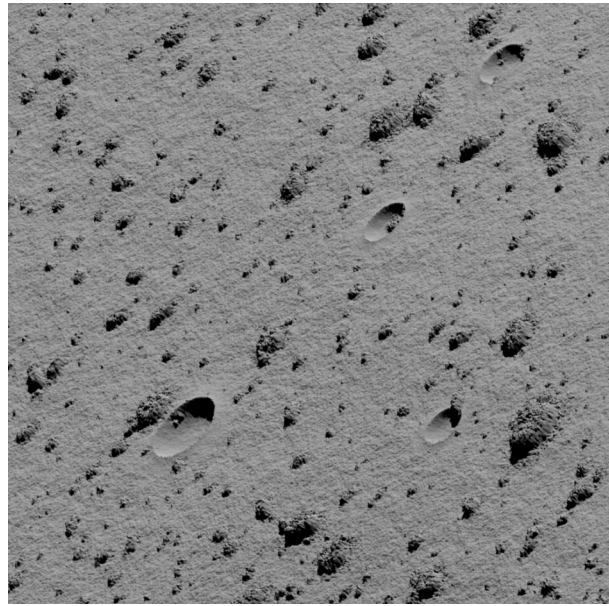


**Figure 10. Central region at 12.5 cm/pixel**

Figure 9 shows a further zoom into the center, this time at 50 cm/pixel, while Fig. 10 reduces this by a factor of four to 12.5 cm/pixel. This technology is being used to study the feasibility of autonomous optical navigation<sup>3</sup> during possible landings on Phobos or other small bodies.

### **Acknowledgements**

This work was carried out at the Jet Propulsion Laboratory, California Institute of Technology, under a contract with the National Aeronautics and Space Administration.

### **References**

- <sup>1</sup>Gaskell, R.W., "Martian Surface Simulations," *Journal of Geophysical Research-Planets*, 98:(E6), 11099-11103, June 25, 1993.
- <sup>2</sup>Gaskell, R., Husman, L.E., Collier, J.B. and Chen, R.L., "Synthetic Environments for Simulated Missions," *IEEE paper 13.0406, IEEE Aerospace Conference, Mar. 2001, Big Sky, MT.*
- <sup>3</sup>Gaskell, R.W., "Automated Landmark Identification for Spacecraft Navigation," *AAS paper 01-422, AAS/AIAA Astrodynamics Specialists Conf., Quebec, 2001.*
- <sup>4</sup>Gaskell (2002), "Determination of Landmark Topography from Imaging Data," *AAS paper 02-021, AAS/AIAA Astrodynamics Specialists Conf., Breckenridge, 2002.*
- <sup>5</sup>Gaskell, R.W., "Optical Only Determination of Small Body Shape and Topography," *ISPRS WG IV/9, Houston, 2003.*
- <sup>6</sup>Gaskell, R.W., "High Resolution Shape and Topography of Eros - Preliminary Results from NEAR Imaging Data," *AGU Spring Meeting, Montreal, 2004.*
- <sup>7</sup>Gaskell, R.W., "Landmark Navigation and Surface Characterization in a Simulated Itokawa Encounter," *AAS paper 05-289, AAS/AIAA Astrodynamics Specialists Conf., Lake Tahoe, 2005*
- <sup>8</sup>Melosh, H.J., "Cratering mechanics - observational, experimental and theoretical," *Annual Review of Earth and Planetary Science*, volume 8, 65-93, 1980.
- <sup>9</sup>Hartmann, W.K. and Gaskell, R.W., "Planetary cratering 2: Studies of saturation equilibrium," *Meteoritics & Planetary Science*, 32:(1), 109-121, January 1997.
- <sup>10</sup>Golombek, M. and Rapp, D., "Size-frequency distribution of rocks on Mars and Earth analog sites: Implications for future landed missions," *Journal of Geophysical Research*, volume 102, 4117-4129, 1997.

<sup>11</sup>Ostro, S.J., Benner, L.A.M., Nolan, M.C., Magri, C., Giorgini, J.D., Scheeres, D.J., Broschart, S.B., Kaasalainen, M., Vokroulicky, D., Chesley, S.R., Margot, J.L., Jurgens, R.F., Rose, R., Yeomans, D.K., Suzuki, S., DeJong, E.M., "Radar Observations of Asteroid 25143 Itokawa (1998SF36)," *Meteoritics and Planetary Science*, 2004.

<sup>12</sup>Thomas, P.C., Binzel, R.P., Gaffey, M.J., Storrs, A.D., Wells, E.N., Zellner, B.H., "Impact Excavation on Asteroid 4 Vesta: Hubble Space Telescope Results," *Science*, Vol 277, 1492-1495, 1997.